JOURNAL OF AIRCRAFT
Vol. 40, No. 2, March–April 2003

Dynamic Stall Control Using a Model-Based Observer

John Magill,* Matthew Bachmann,† and Gregory Rixon‡
Physical Sciences, Inc., Andover, Massachusetts 01810-1077
and
Keith McManus§
General Electric Corporate R&D Center, Niskayuna, New York 12309

Dynamic stall control is of interest for its potential to enhance the performance of rotorcraft. The experiments described used pulsed vortex generator jets, shown previously to prevent separation on steady wings and airfoils, to delay dynamic stall on a rapidly pitching airfoil. In tests performed on a NACA-0012 airfoil at low Reynolds numbers, the jets yielded a 25–35% increase in the lift coefficient achievable without moment stall. Next, a differential equation model of the dynamic stall process was derived and experimentally validated. Models of this form enable the application of well-known control theory to the design of flow control systems. In the final round of experiments, a state observer based on the mathematical model detected incipient dynamic stall. A controller used the stall prediction to operate the pulsed jets only when needed to prevent stall. The controller turned the jets off for the remainder of the oscillation cycle. The controller only operated the jets for about 25% of the pitch cycle, so that the best lift increases of the early experiments could be achieved with only 25% of the air mass flow.

Nomenclature

$\boldsymbol{A}, \boldsymbol{B}, \boldsymbol{C}$	=	parameter matrices in standard linear model form
B	=	separation state in mathematical model
$B_s(\alpha)$	=	steady separation functions
C_μ	=	jet momentum coefficient
c	=	airfoil chord
D	=	jet diameter
f_p	=	jet pulsing frequency
k_-	=	constant parameters in model
$\boldsymbol{L}$	=	Luenberger gain matrix
N	=	number of jets
P_2	=	pressure at second tap from leading edge
S	=	model planform area
Sr_c	=	chord-based Strouhal number
U_∞	=	freestream velocity
$\boldsymbol{u}$	=	input state vector in standard linear model form
$\boldsymbol{X}$	=	state vector in standard linear model form
$\boldsymbol{Y}$	=	output vector in standard linear model form
Z	=	lift or pressure state in mathematical model
$Zs(\alpha)$	=	steady pressure or lift
α	=	angle of attack
$\Gamma^*(\alpha)$	=	nominal steady circulation function
Δ	=	jet duty cycle
ω	=	pitch cycle frequency
$\bar{\omega}$	=	reduced pitch cycle frequency

Superscripts

$\hat{}$	=	observer estimates
$\cdot$	=	time derivative

Received 24 March 2002; revision received 1 October 2002; accepted for publication 4 October 2002.

*Principal Research Engineer. AIAA Member.
†Summer Co-op Student.
‡Summer Co-op Student.
§Mechanical Engineer. AIAA Member.

Introduction

THE work described in this paper extends previous results in pulsed-jet separation control over stationary airfoils to the problem of dynamic stall. The actuators, pulsed vortex generator jets (PVGJs), consist of discrete circular air jets on the upper surface of the airfoil. The jets produce vortices that promote mixing, energize the boundary layer, and prevent separation. Experiments with these actuators on stationary wings and airfoils show that an increase in the lift coefficient can be achieved by preventing upper-surface separation.[1–6] The experiments described here show that PVGJs are equally effective at preventing dynamic stall.

Of equal significance is a set of mathematical results that show how to describe the dynamic stall process in a nonlinear state-space model. Experiments show that a controller based on the new mathematical model can reduce the air supply required for the jets by using them only when stall is imminent.

The remainder of this section describes PVGJs and the dynamic stall problem in more detail. Later sections will describe the experimental apparatus, the mathematical model, and experimental stall control results. Several other researchers have explored other techniques for controlling dynamic stall.[7–12] Although the experiments described here focused only on PVGJs, the observer-based approach can be applied to the operation of many other flow control actuators.

Benefits of Dynamic Stall Prevention

The performance of a rotorcraft is ultimately limited by the blade's ability to produce lift. In general, lift increases as the blade angle of attack increases, but this trend is reversed at higher angles of attack because of flow separation (stall) on the blade upper surface. A rapidly pitching blade can reach higher angles of attack without separation than a blade pitching up slowly. The rapidly pitching blade, thus, can produce a higher maximum lift coefficient. This dynamic pitch advantage is due to the time required for separation to occur.

When the blade finally does stall in rapid pitch up, a strong vortex is shed from the leading edge. The vortex and its associated low-pressure region propagate over the upper surface and produce violent transient loads, in particular a large nose-down pitching moment and a brief lift increase. This process is known as dynamic stall. The transient loads result in large vibrations that can be catastrophic for blade structures.

Rotorcraft, by their nature, are positioned to take advantage of the increased peak lift on a rapidly pitching airfoil. In forward flight, the retreating-side rotor blade experiences a lower relative wind speed

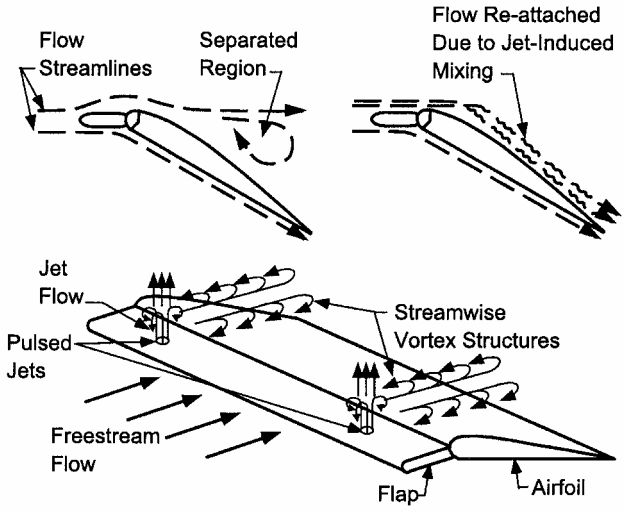

Fig. 1 PVGJs create mixing structures that prevent flow separation.

than the advancing blade. To balance the distribution of lift over the rotor disk, the retreating blade must have a higher lift coefficient than the advancing blade, and this is accomplished by pitching the blades up as they retreat.

The limit on lift coefficient constrains the mean lift that the rotor can produce. This limits load capacity and forward flight speed because rotor lift must equal vehicle drag in forward flight. For a particular mean lift, stall also limits the difference between the maximum and minimum lift coefficient over all rotor azimuth angles. This also limits forward flight speed because it constrains the ability to balance the net lift between advancing and retreating blades. Both forward flight speed and load capacity could be increased if the pitching blades could produce higher lift coefficients without the danger of dynamic stall. This research was aimed at using pulsed air jets on an airfoil upper surface to prevent dynamic stall.

PVGJ Actuators

The principle of operation for the PVGJ is shown in Fig. 1. Separation occurs on an airfoil when kinetic energy of the air in the boundary layer is depleted by viscous shear with the surface. The energy depletion is exacerbated by the strong adverse pressure gradient that exists on an airfoil upper surface just behind the leading-edge suction peak. When flow separates on an airfoil upper surface, drag rises, lift decreases, and a strong nose-down pitching moment develops.

PVGJs generate vortices that promote mixing of high-energy freestream air into the boundary layer to displace low-energy fluid. This keeps the boundary layer from separating and allows operation at higher angles of attack, resulting ultimately in higher lift and lift-to-drag ratio. McManus and Magill[6] showed earlier that PVGJs can increase the maximum lift on a flapped NACA 4412 by more than 25%. Prior work by Physical Sciences, Inc.,[1–6] and other research groups[10] has also shown that pulsed jets are more effective at preventing separation than steady jets.

In the subsequent discussion, the operating conditions of pulsed jets are characterized using four parameters found to be important in previous studies. They are velocity ratio, duty cycle, Strouhal number, and momentum coefficient. The velocity ratio (VR) is the ratio of jet exit velocity to the wind-tunnel freestream velocity. The duty cycle Δ is the fraction of the jet-pulse cycle during which the jet is flowing and is given as a percentage. The Strouhal number Sr_c is defined by the relationship

$$Sr_c = f_p c / U_\infty$$

where f_p is the PVGJ pulse frequency in hertz. The momentum coefficient indicates the mass of air flowing through the jets and is defined as

$$C_\mu = \mathrm{VR}^2 \times (\pi D^2/4S) \times \Delta \times N$$

This quantity is useful for comparison to other flow control methods published by other researchers.

Prior work with flat plates and airfoil sections[2–5] has shown that a particular range of parameters generally provided optimum separation control effect. Peak lift enhancement generally occurs near a Strouhal number $Sr_c = 0.5$ for static airfoils. However, for dynamic pitching, prior work has shown that higher frequencies are necessary so that many jet pulses are produced during a pitch-up.

The effectiveness of the jets generally increases with velocity ratio until a maximum performance is reached. Further increase in VR has no effect. Lift enhancement generally saturates in this way when the velocity ratio is increased beyond VR = 4. Prior investigations also showed that duty cycles of 25% produce the same effect as those of 50% for a given VR. Thus, lower duty cycles are typically chosen as they require less air supply.

Experimental Facility

Wind Tunnel

All of the experiments were conducted in a low-speed Eiffel-type wind tunnel with a 30×30 cm test section. It is capable of producing velocities up to 60 m/s in the test section. However, for these experiments, the speed was limited to 15 m/s so that higher dimensionless pitch rates could be achieved.

The tunnel was equipped with a pitch drive system. This device employed a brushless motor, connected to the model through a bell crank, to pitch the model. The model pivoted on a set of ball bearings at the drive side of the test section and in a bushing in the test section wall opposite the drive. The motor was capable of torques up to 7 N · m (1000 oz · in.). A personal computer-based motion control system produced motions with desired rates and angular excursions. For the experiments at hand, all motions were sinusoidal. A graphical user interface allowed the operator to specify the frequency, amplitude, and mean pitch angle for the motion. Figure 2 shows the pitch drive system installed in the wind-tunnel test section.

Model

The wind-tunnel model was a NACA-0012 airfoil section that spanned the entire test section. The model had a chord length of 15 cm and was tested at a Reynolds number of 1.7×10^5. It was formed from a plywood rib and spar frame, with a thin plywood skin covered with an iron-on plastic coating to provide a smooth surface. A rough strip (100-grit sandpaper) was installed at the leading edge to force transition to turbulent flow. The layout of the model is shown in Fig. 3.

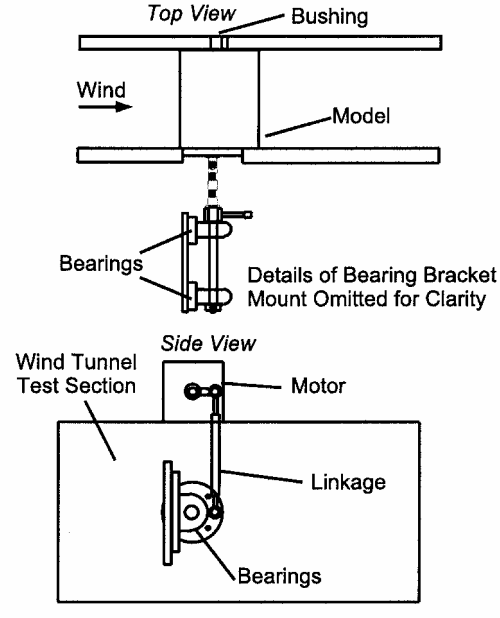

Fig. 2 Dynamic pitch drive.

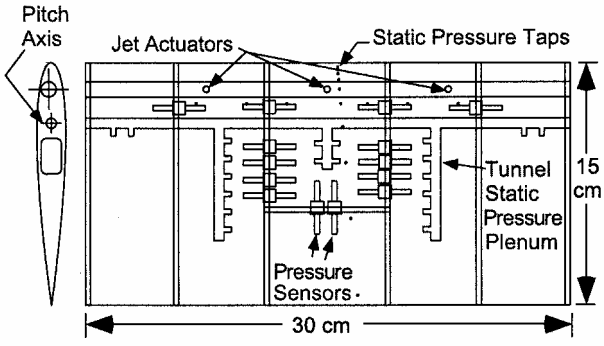

Fig. 3 Blade section model for dynamic stall control experiments, pressure sensor tubing omitted for clarity.

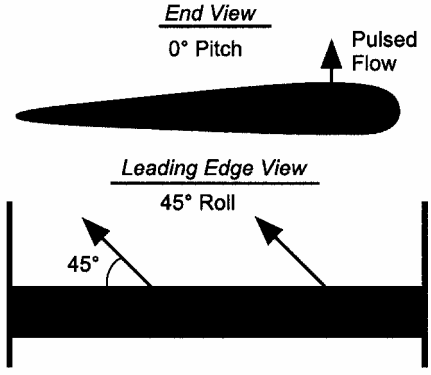

Fig. 4 Orientation of pulsed jets.

The model was instrumented with fast-response micromachined differential pressure sensors to measure the pressure distribution the upper surface of the airfoil. The taps were arranged in a single chordwise row and a spanwise row. Because the airfoil was symmetric, lower surface pressures could be measured by repeating pitching experiments at negative angles of attack. The pulsed jets affect the upper surface almost exclusively, so that the lower surface pressures were assumed to be identical with and without jets operating.

The sensors had a time constant less than 1 ms, a full-scale range of 2000 Pa (0.3 psi differential), and a reported accuracy of 0.5% full-scale. One port for each sensor was attached to the static port on the tunnel pitot–static probe. Lift and pitching moment were computed from a trapezoidal-rule integral of the measured pressures. As a result, the lift coefficient could be determined to within 0.18 and pitching moment coefficient to an accuracy of 0.02.

An airfoil model that fully spans a test section is typically taken to represent a two-dimensional flow environment. We note, however, that the discrete jets produce a three-dimensional flowfield. Thus, the model represents not a two-dimensional blade section but a finite span blade segment. Forces on the blade are measured from a distribution of pressure taps on the blade surface. The measured loads are considered to be representative of the mean blade section properties.

The leading edge of the model was fitted with three PVGJs. The jets were pulsed from a solenoid valve at the airfoil root. For the purpose of discussion, jets on refers to the condition where the jets are pulsing periodically, and jets off refers to the condition where they are not pulsing. The terms on and off do not refer to the individual portions of the jet pulse cycle where air is or is not flowing.

Air was delivered from the valve to the jets through a brass tube along the leading edge. As shown in Fig. 4, the jets were pitched 90 deg to the model chord and rolled 45 deg to the right. The flow of air to the jets was metered using a mass flow controller. The controller required several seconds to reach a steady operating condition, making it impossible to turn the jets on and off quickly with a known mass flow. Because the closed-loop controller needed to turn them on and off during a single pitch oscillation, a dual valve system was devised. One valve was located in the model, and the other dumped air outside of the tunnel. When the controller turned the jets on, the valve in the tunnel pulsed. To turn the jets off, the tunnel valve was closed, and the dump valve pulsed. Thus, the mass flow controller always provided a constant flow through a pulsing valve. The controller either diverted the air to the PVGJs or to the dump valve.

Without the diverting valve, pressure builds in the supply line, and the first few pulses after the controller turns the jet on are much stronger than those produced in steady pulsed operation. Because the goal of the experiments was to evaluate control schemes where the jet pulsing might be started during the cycle against constant-pulsing operation, it was necessary to implement a method of ensuring constant jet operation. It is an artifact of the tests at hand, and will not be required when PVGJs are installed on a flight vehicle. Operating on a rotorcraft, the jets could be run from a pressurized line, and some variation in jet velocity could be tolerated.

Procedure for Stall Control Performance Measurement

The desired result of dynamic stall control is that we achieve the high peak lift possible on a rapidly pitching airfoil without the undesirable nose-down pitching moments that accompany the passage of the stall vortex. The metric for evaluating the baseline and controlled airfoils was the maximum stall-free lift coefficient (MSLC). If lift is monotonically increasing with pitch angle, then the metric is equivalent to measuring the maximum stall-free pitch angle.

For any particular test condition, measurement of the MSLC began with a small-amplitude oscillation from a pitch angle $\alpha = 0$ to a selected maximum. For each oscillation, the pitching moment and lift coefficient were recorded as a function of time. If the moment did not exhibit the excursion that characterizes dynamic stall, the experiment was repeated with a higher pitching motion amplitude. The maximum angle was typically increased by 1 deg. The process was repeated until the moment trace showed features associated with the shedding of the dynamic stall vortex, that is, moment excursion. The maximum lift coefficient attained on the run before the one where stall appeared was designated the MSLC. To reduce the noise in measurements, 50 pitch cycles were executed at each condition. The data reported later represent ensemble averages of the 50 cycles.

Pitch rates in the experiments were characterized by the dimensionless parameter $\bar{\omega}$ defined by

$$\bar{\omega} = \omega c / U_\infty$$

where ω is the cyclic pitch frequency in radians per second.

Open-Loop Stall Control Experiments

Three separate experiments comprised the demonstration of jet effectiveness. The first identified the MSLC for the airfoil without the jets operating. It began with a small pitch excursion: 0–7 deg. The excursion was extended until dynamic stall occurred, identified by a departure in pitching moment. This experiment identified the baseline for the given frequency. In the second experiment, the jets were turned on. The experiment was repeated to identify jets-on MSLC and, hence, the jet-extended pitch range. In these experiments, the jets were operated at a duty cycle $\Delta = 30\%$, $\mathrm{VR} = 8.4$, and pulse frequency of $Sr = 2.0$. Finally, an excursion to the jet-extended range was repeated, but without operating the jets. This demonstrated the severity of stall that would occur without the jets.

Figures 5 and 6 show pitch and moment curves for two pitch frequencies. At $\bar{\omega} = 0.05$, the jets extended the stall-free range nearly 3 deg. The resulting increase in peak lift was 25%. At $\bar{\omega} = 0.1$, the range was extended 4 deg, resulting in a 35% increase in peak lift.

Controller Design

Preceding sections presented evidence that pulsed jets can prevent dynamic stall over pitching airfoils, resulting in increased peak lift. In the experiments described earlier, the jets were operating constantly. In practice, however, auxiliary air and energy to operate flow control devices are limited on flight vehicles. When an active control strategy is applied, it is possible to achieve the same effect

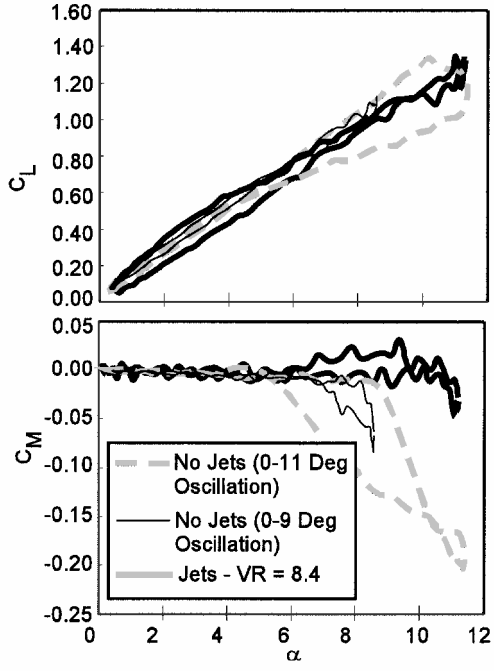

Fig. 5 Pulsed jets delay dynamic stall on NACA-0012 airfoil at $\bar{\omega}$ = 0.1; jet conditions: f_p = 200 Hz, VR = 8.4, and Δ = 30%.

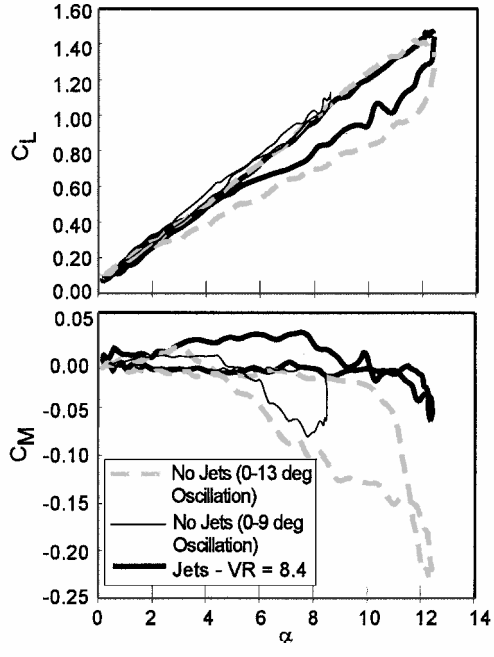

Fig. 6 Pulsed jets extend pitch range on NACA-0012 airfoil at $\bar{\omega}$ = 0.05; jet conditions: f_p = 200 Hz, VR = 8.4, and Δ = 30%.

as continuous operation while only operating the jets on a portion of the pitch cycle.

The stall process begins at different angles of attack for different pitch rates and amplitudes. Rather than attempting to perform a wide range of experiments to construct a jet operation schedule, we present here a model-based approach that determines when jets should be turned on. The algorithm is fairly simple but can be applied to any range of operating condition for which the model is valid.

Mathematical Model

The closed-loop control system employed an observer that detected imminent separation using feedback from a single upper surface pressure sensor and a measurement of the pitch angle of the airfoil. The observer was based on a mathematical model of the unsteady aerodynamics of the airfoil. The stall detection model allowed the controller to operate the jets only when needed to prevent stall, dramatically reducing jet air requirements over the constant-pulsing operation.

The model structure can be applied to predict either total lift or pressure at a specified location given the pitch time history. The total lift produced by an airfoil is closely related to the strength of the upper surface pressure field, making this interchange possible. Because the greatest variations in pressure occur in the leading edge (LE) suction peak, the pressure at the second chordwise tap from the LE, P_2, was determined to be the best control metric for the present model. Hence, the model was applied to the modeling of P_2.

Although the details of the flow physics were not used to derive the model, three mechanisms involved in the flow dynamics were given consideration. First, the model solution was required to relax to the steady pressure solution at a steady pitch angle. Second, because lift (integrated pressure) is known to be proportional to circulation around an airfoil and because circulation is added to the flow as the wing pitches, a term resembling this circulation addition was included. Finally, two different mechanisms were provided for the relaxation from transient to steady pressure, depending on angle of attack. This resembles the behavior of the physical system as well (Fig. 7). At low angles of attack (Fig. 7a), the flow around an airfoil transitions from one steady flow condition to another through convection, pressure transients, and the shedding of a starting vortex, but without a large separation over the upper surface. At high angles of attack (Fig. 7b), this transition is characterized by the shedding of a dynamic stall vortex (DSV).

The model contained three states:

$$Z = \text{lift or pressure at a point}$$
$$B = \begin{cases} 0, & \text{fully attached flow} \\ 1, & \text{fully separated flow} \end{cases}$$
$$\dot{B} = \frac{\mathrm{d}B}{\mathrm{d}t} \tag{1}$$

The separation dynamics consisted of a second-order relaxation to the steady separation condition:

$$\ddot{B} = K_B[B_s(\alpha) - B] - K_{\dot{B}}\dot{B} \tag{2}$$

where K_B is a constant and $K_{\dot{B}}$ is the damping parameter. The second-order model of separation dynamics was chosen as a means of producing the peak in both lift and suction observed when the DSV is shed. As shown in Fig. 8, the damped second-order model

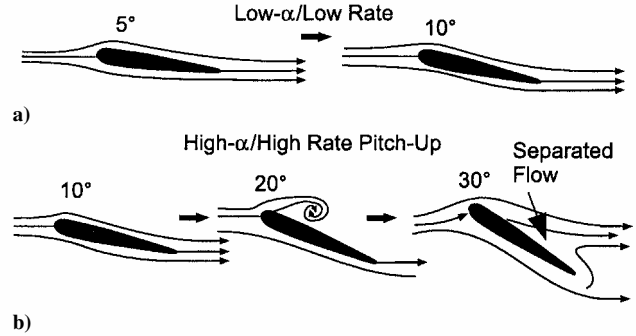

Fig. 7 Two mechanisms permit transition between steady flows at different angles of attack: a) low angle of attack and b) high angle of attack–dynamic stall vortex.

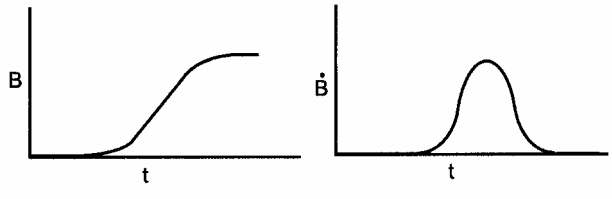

Fig. 8 Damped second-order system provides peak associated with dynamic stall vortex; response of B and $\dot{B}$ to a step change in $B_s(\alpha)$.

provides a smooth transition to a steady separation condition on a sudden pitch change, and the derivative of B appears as an isolated peak. A brief rise in suction and lift is typically observed when a dynamic stall vortex is shed. When a term proportional to $\dot{B}$ is added to the lift/pressure, the DSV shedding effect can be included. To cause the DSV to appear at only higher angles of attack, $B_s(\alpha)$ can be forced to remain zero at low angles of attack (known to be the case) so that no separation occurs at all in that region.

Although the steady separation is buried in the model as a result of including the static characteristic function $B_s(\alpha)$, the model does not assume that the steady and dynamic stall processes are similar. The steady separation function applies only to the steady airfoil. In the present model, the dynamic stall process is represented by the nonzero derivative of B during the change from unstalled to stalled flow. The static stall function indicates when the dynamic stall process, that is, vortex shedding, is necessary to move from some instantaneous unstalled (and unstable) condition to a steady, stable, stalled flow.

The pressure dynamics are first order and the state equation consist of three terms:

$$\dot{Z} = \underbrace{K_Z[Z_s(\alpha) - Z]}_{\text{convective relaxation}} + \underbrace{\frac{\partial \Gamma^*(\alpha)}{\partial \alpha}\dot{\alpha}}_{\text{circulation addition}} + \underbrace{K_{Z/B}\ddot{B}}_{\text{DSV shedding influence}} \tag{3}$$

The first term, wherein K_Z is a constant parameter defining the speed of the lift dynamics and $Z_s(\alpha)$ is the steady pressure curve for the location of interest, produces the relaxation to the steady condition. The second term accounts for the addition of circulation when the model is pitched. $\Gamma^*(\alpha)$ is called the nominal circulation function. It is determined empirically for a specific airfoil. The third term produces the transient rise in Z resulting from the separation dynamics. Because $\dot{Z}$, not Z, appears on the left-hand side, $\ddot{B}$ is added on the right. The result will be a term proportional to $\dot{B}$ in Z. Although $\ddot{B}$ is not a state, it can be written in terms of the state variables as shown in Eq. (2). $K_{Z/B}$ is a constant relating separation effects to Z.

Although this model was derived independently, it is, in some ways, similar to a dynamic stall model derived by Petot at ONERA.[13] Peters[14] also demonstrated that the ONERA model could be augmented and used for large-amplitude motions such as those of interest here. Because it was designed to predict resultant loads, it is not known how well the ONERA model predicts pressure at a point on the wing.

The nature of our model lends itself to the application of conventional control methods. It consists of a third-order linear state model with known nonlinear feedforward terms. There are no transport lags within the model, and the stall delay is modeled by the second-order lag in the B dynamics. The structure made it possible to construct the state observer that was used in the closed-loop control design.

Simulation and Model Validation

The model response was compared to experimental data for a pitch-up maneuver to tune the model. The model was used as the basis for a MATLAB®/SIMULINK simulation of the wing aerodynamics. Several combinations of steady separation and nominal circulation functions, as well as several variations in the constant parameters, were tried until a good match was obtained. The simulation was performed by measuring a pitch angle time history from an experiment and applying it as an input to the simulation. The simulated P_2 was compared to that measured in the experiment.

Figure 9 shows the steady lift and separation functions and the nominal circulation used in the simulation of the airfoil model. The steady pressure function was measured experimentally by moving the model very slowly over a range of angles. Because this work focused on oscillatory pitching motions relevant to rotorcraft, the simulation included hysteresis in $Z_s(\alpha)$, which appeared in the measured curves.

The separation function begins to increase at the point where the steady pressure curve begins to bend, consistent with the onset

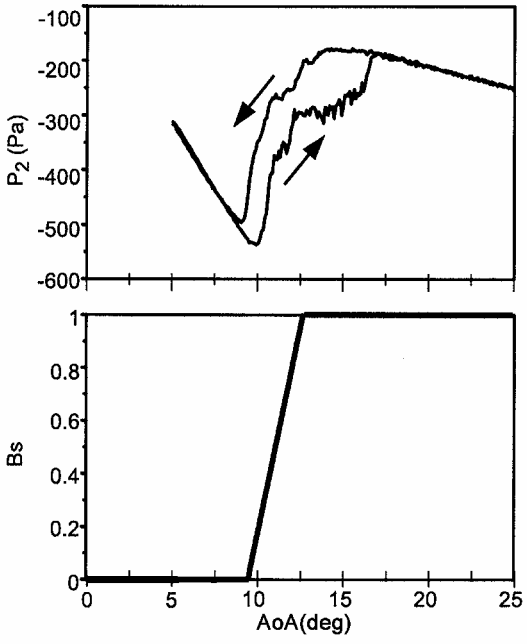

Fig. 9 Steady lift and separation functions used in airfoil model.

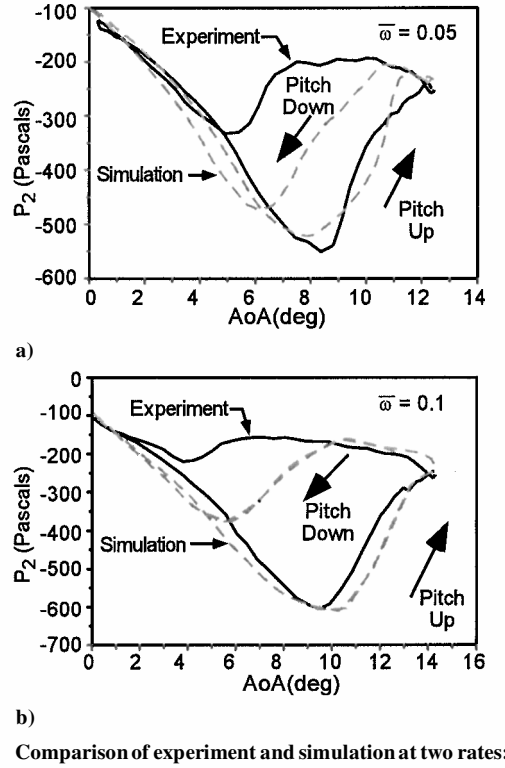

Fig. 10 Comparison of experiment and simulation at two rates: a) $\bar{\omega}$ = 0.05 and b) $\bar{\omega}$ = 0.1.

of stall. It remains zero at low angles of attack, where the flow is attached. The nominal circulation slope $\partial\Gamma^*/\partial\alpha$ was chosen to make the model match the slope of the pressure function $Z_s(\alpha)$ in the prestall region. The function $\Gamma^*(\alpha)$ does not appear in the model; only its derivative is required. We assumed it to have a linear structure, so that its slope is simply a constant.

The parameters used to model the airfoil at hand were $K_z = 120$, $K_B = 1000$, $K_{\dot{B}} = 140$, $K_{Z/B} = -6$, and $\partial\Gamma^*/\partial\alpha = -55$. The steady P_2 curve was used at $Z_s(\alpha)$. Figure 10 compares the simulation to two experiments conducted at different reduced pitch rates. Agreement is good for the pitch-up, though some discrepancy exists in the pitch-down.

For the present purposes, it is sufficient to predict the onset of stall so that the jets can be turned on. Thus the discrepancy between

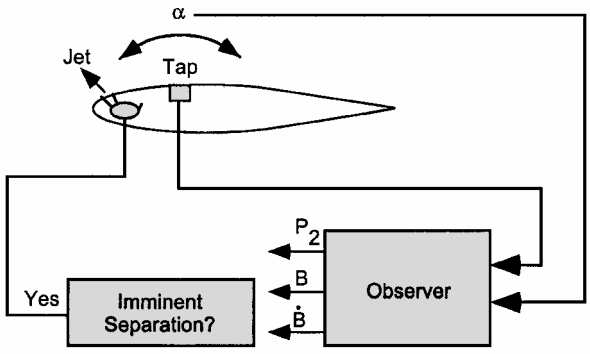

Fig. 11 Closed-loop dynamic stall control system.

model and experiment in the reattachment period does not hamper controller performance. Future applications may require that the reattachment model be improved, particularly if the model is to be used to analyze rotor blade structural dynamics.

Control Algorithm

The controller designed for these tests detected imminent stall and activated the pulsed-jet actuators to prevent separation. The controller also switched the jets off once separation was no longer a danger. The algorithm is shown in Fig. 11. The decision to turn on the jets was based on the B state variable in a model of the unsteady aerodynamics operating in real time on the control microprocessor. At each sampling time, the separation is projected ahead to the next sampling instant using the current estimates of B and its derivatives. If B is predicted to cross a preset threshold ($B = 0.5$), the jets are turned on. The jets are turned off once the airfoil begins the pitch down.

Because B cannot be measured, it must be determined from other measurements. For a suitable linear model with known inputs and a measurable output, the internal states can be determined using a Luenberger observer (see Refs. 15 and 16). This controller requires that the angle of attack is known at any instant. The limitations of this requirement are addressed later.

The observer correlates the behavior of states with measurable quantities using a system of differential equations. Thus, even though the stall process begins behind the suction peak and is well underway once the pressure peak begins to dissipate, a measurement of the suction in the peak can be used to determine when the wing is near stall. The suction peak, P_2, was chosen over another sensor because this region of the airfoil undergoes the largest changes in pressures during a pitch cycle, providing good sensitivity to changes in the flow.

The controller was implemented on a personal computer with an analog data acquisition board. The board generated a 200-Hz timing signal that was used to trigger its analog input conversion circuit. The control software waited at each sampling interval until the triggered A/D conversion was complete. It then read the A/D values and used them to perform control decisions.

The pitch rate was estimated from pitch angle feedback by digitally filtering a backward difference. In searching for the beginning of pitch-down, where the jets are switched off, a decrease of pitch angle over a 10 time-step range was required. This prevented noise-induced switch off.

Luenberger Observer

The observer employed the model of the aerodynamic system operating in parallel with the controlled system. The output of the model was compared with a measured system output. The model states, which are the estimates of the system states used by the controller, are updated based on the error between the measured (actual) and model outputs. The observer structure is shown in Fig. 12. Stability properties for the Luenberger observer and constraints on the gain matrix may be found in most control system text books (see Refs. 15 and 16).

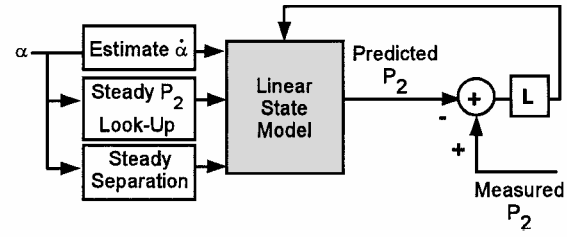

Fig. 12 Luenberger observer for dynamic stall control.

To implement the observer, the state equations were written in the form

$$\dot{\boldsymbol{X}} = \boldsymbol{AX} + \boldsymbol{BU}, \qquad \boldsymbol{Y} = \boldsymbol{CX} \tag{4}$$

where $\boldsymbol{X}$ is the state vector, $\boldsymbol{U}$ is the input, and $\boldsymbol{Y}$ is the output.

When these equations are compared to Eqs. (2) and (3), the input vector $\boldsymbol{U}$ can be replaced with

$$\boldsymbol{U} = \begin{bmatrix} Z_s(\alpha) \\ B_s(\alpha) \\ \dot{\alpha} \end{bmatrix} \tag{5}$$

and the state $\boldsymbol{X}$ with

$$\boldsymbol{X} = \begin{bmatrix} Z \\ B \\ \dot{B} \end{bmatrix} \tag{6}$$

The state model matrices are

$$\boldsymbol{A} = \begin{bmatrix} -K_Z & -K_{Z/B}K_B & -K_{Z/B}K_{\dot{B}} \\ 0 & 0 & 1 \\ 0 & -K_B & -K_B \end{bmatrix}$$

$$\boldsymbol{B} = \begin{bmatrix} K_z & K_{Z/B}K_B & \dfrac{\mathrm{d}\Gamma^*}{\mathrm{d}\alpha} \\ 0 & 0 & 0 \\ 0 & K_B & 0 \end{bmatrix}, \qquad \boldsymbol{C} = [1 \quad 0 \quad 0] \tag{7}$$

These equations were discretized for implementation on a digital control platform. The discrete time observer, executed at each time step n, was implemented in three steps. First, the input vector $\boldsymbol{U}$ was constructed. Next, the state estimate $\boldsymbol{X}$ was updated using the relation:

$$\hat{\boldsymbol{X}} = \boldsymbol{A}\hat{\boldsymbol{X}}_n + \boldsymbol{BU}_n + \boldsymbol{L}(y - \hat{y}) \tag{8}$$

The matrix L is a gain matrix whose values govern the convergence properties for the observer. Finally, the model output was computed:

$$\hat{y} = \boldsymbol{CX} \tag{9}$$

The estimates of B and $\dot{B}$ were then used by the control decision algorithm.

One deficiency of this approach is that it requires measurements of the angle of attack. For a rigid rotor the angle of attack could be computed from rotor actuator commands and velocity information estimated within the flight control computer. For the realistic elastic rotor, structural dynamics must be included in the rotor blade model. Although these complexities may appear difficult, they will need to be overcome for any complex active rotor control system whether it employs pneumatic control or active structural elements. An alternative approach is to seek a model that uses feedback from multiple pressure sensors to obviate the need for the α measurement.

Closed-Loop Stall Control Experiments

A few cases from the pulsed-jet experiments described were repeated using the closed-loop control system. Figures 13 and 14 compare the closed-loop control performance to the results produced by operating the jets throughout the cycle. The behavior of the wing without jets is shown for reference. At both $\bar{\omega} = 0.05$ and $\bar{\omega} = 0.10$, the closed-loop control is as effective at preventing stall as the continuously pulsing jets. The jets, however, are only operated for 25% of the pitch cycle under the command of the controller. The points at which the jets are switched on and off are indicated in Figs. 13 and 14. Because Figs. 13 and 14 were constructed by averaging several cycles, the switch points are indicated at the point where half of the runs in the average switched.

Only the $\bar{\omega} = 0.05$ run (Fig. 14) shows some moment excursion during the pitch cycle with closed-loop control. This near stall, however, occurs on the downward pitch. If the jets are used to prevent stall and are switched off at the maximum angle, then dynamic stall can still begin on the pitch-down if the airfoil remains above the static stall angle for sufficient time. This did not occur for the $\bar{\omega} = 0.1$ case. This pitch-down stall can be prevented if the jets remain on during the first portion of the pitch-down as was proven in the cases where jets operate over the full cycle.

The controller turned the jets on at a lower angle during the $\bar{\omega} = 0.05$ motion than in the $\bar{\omega} = 0.1$ motion. This was necessary because at the lower pitch rate the airfoil stalls at a lower angle of attack. This indicates that the controller model has indeed captured the essential features and timescales of the flow dynamics.

Figure 15a compares the observer output to the measured system output, the pressure at the second tap. Figure 15a was constructed

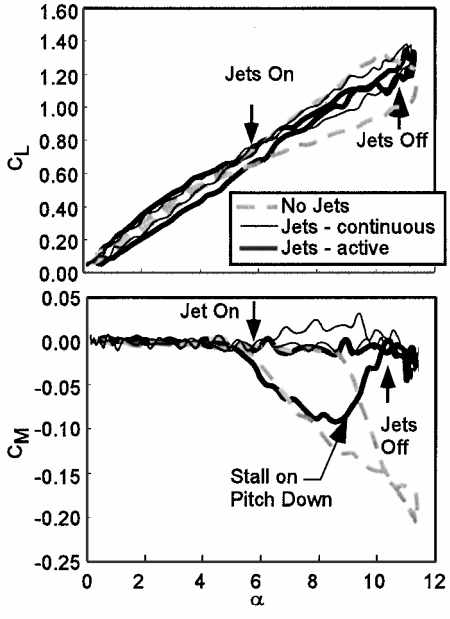

Fig. 13 Closed-loop controller delays stall with greatly reduced mass flow $\bar{\omega}$ = 0.05 Hz; jet conditions: f_p = 200 Hz, VR = 8.4, and Δ = 30%.

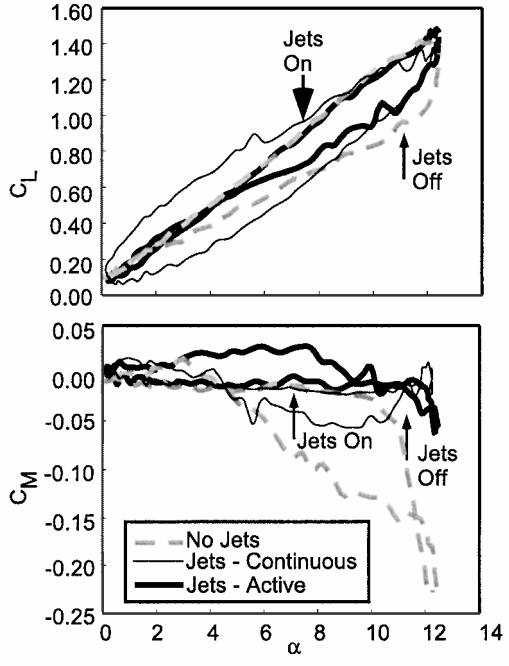

Fig. 14 Closed-loop controller delays stall with greatly reduced mass flow $\bar{\omega}$ = 0.1 Hz; jet conditions: f_p = 200 Hz, VR = 8.4, and Δ = 30%.

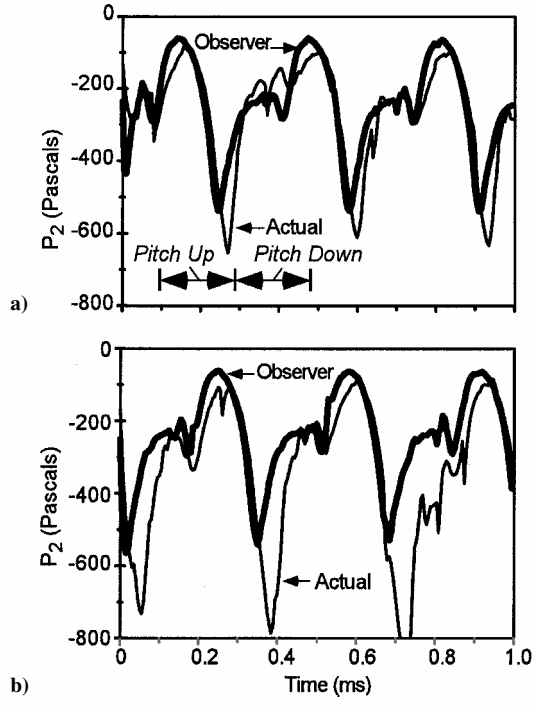

Fig. 15 Comparison of measured pressure to observe estimates: a) no jets and b) jets actively controlled.

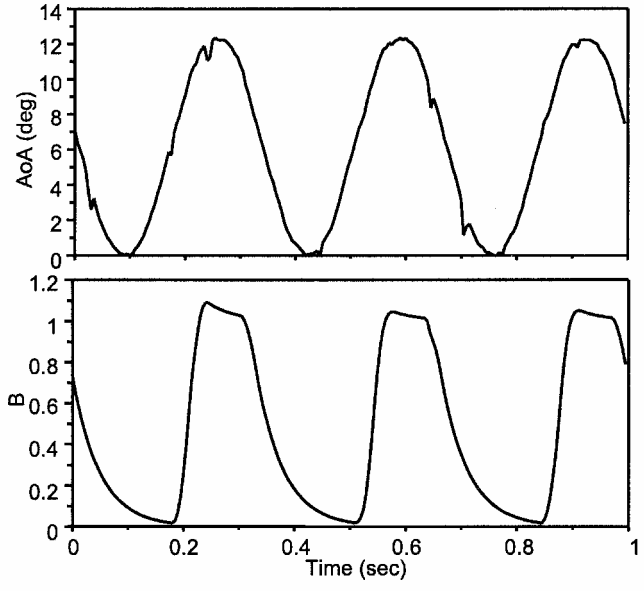

Fig. 16 Estimated separation during pitching experiments; angle of attack shown for reference.

from data acquired without the jets in operation. The observer converged quickly after it is switched on and continued to match the system output.

Figure 15b compares the observer and system output while the active control system is activating the jets. The observer continued to track the actual output for the part of the cycle while the jets are off. For the portion of the cycle where the jets are operating, the observer's model did not match the actual dynamics because the jets significantly alter the airfoil characteristics. However, this did not diminish controller performance because the control criterion is only in effect when the jets are off. Once the jets were on, no state-based control decision was made until after the jets were turned off at the top of the pitch cycle. It is possible to account for the error by augmenting the model to switch between a case tuned to the basic airfoil and one tuned to the airfoil with jets, but such activity was not required for this demonstration.

Figure 16 shows the observer-estimated value of B during the pitch cycle at $\bar{\omega} = 0.1$. The angle of attack is shown for comparison. The control system was active in this experiment.

Summary

The experiments just described demonstrated that PVGJs can increase the peak lift that can be produced by an oscillating blade section without incurring the violent pitching moment excursions that result from dynamic stall. Peak lift increases as large as 35% were achieved when the jets were pulsed continuously while the airfoil pitched cyclically.

To reduce the airflow required to realize the benefits of PVGJs, a closed-loop controller was implemented. The controller used a model-based observer to detect imminent separation and then operated the jets only on the portion of the pitch cycle where a stall risk was identified. In demonstration experiments, the controller was able to achieve the same lift benefits possible with open-loop pulsing (a 25–35% increase), but the jets were only operated on one-fourth of the pitch cycle. This corresponds to 90 deg of rotor azimuth. The closed-loop system used 75% less air than the open-loop system.

This research demonstrates the importance of developing control-oriented mathematical models. As the aerodynamic components of flow control technology mature, it will be necessary to marry the actuators with control algorithms that maximize their capabilities. The body of literature in the field of nonlinear control is rich with model-based techniques that can be applied to aerodynamic systems. Model development is a key step in making use of these algorithms.

These experiments were conducted in low Reynolds number incompressible flows. It is now necessary to demonstrate PVGJ dynamic stall control in compressible flows more closely resembling the environment around a helicopter rotor.

Acknowledgments

This work was supported by NASA Ames Research Center under a Phase I Small Business Innovation Research Contract NAS2-98061. The Contract Monitor was Thomas Norman.

References

[1]Magill, J. C., and McManus, K. R., "Exploring the Feasibility of Pulsed Jet Separation Control for Aircraft Configurations," *Journal of Aircraft*, Vol. 38, No. 1, 2001, pp. 48–56.

[2]McManus, K. R., Davis, S. J., and Legner, H. H., "Pulsed Vortex Generator Jets for Active Control of Flow Separation," AIAA Paper 94-2218, June 1994.

[3]McManus, K. R., Joshi, P. B., Legner, H. H., and Davis, S. J., "Active Control of Aerodynamic Stall Using Pulsed Jet Actuators," AIAA Paper 95-2187, June 1995.

[4]McManus, K. R., Ducharme, A., Goldey, C., and Magill, J., "Pulsed Jet Actuators for Suppressing Flow Separation," AIAA Paper 96-0442, Jan. 1996.

[5]McManus, K. R., Magill, J., "Airfoil Performance Enhancement Using Pulsed Jet Separation Control," AIAA Paper 97-1971, July 1997.

[6]McManus, K., and Magill, J., "Separation Control in Incompressible and Compressible Flows Using Pulsed Jets," AIAA Paper 96-1948, June 1996.

[7]Carr, L. W., and McAlister, K. W., "The Effect of Leading-Edge Slat on the Dynamic Stall of an Oscillating Airfoil," AIAA Paper 83-2533, Oct. 1983.

[8]Carr, L. W., Chandrasekhara, M. S., Wilder, M. C., and Noonan, K. W., "The Effect of Compressibility on Suppression of Dynamic Stall Using a Slotted Airfoil," AIAA Paper 98-0332, Jan. 1998.

[9]Chandrasekhara, M. S., Wilder, M. C., and Carr, L. W., "Unsteady Stall Control Using Dynamically Deforming Airfoils," *AIAA Journal*, Vol. 36, No. 10, 1998.

[10]Greenblatt, D., and Wygnanski, I., "Dynamic Stall Control by Oscillatory Forcing," AIAA Paper 98-0676, Jan. 1998.

[11]Acharya, M., and Metwally, H., "Unsteady Pressure Field and Vorticity Production over a Pitching Airfoil," *AIAA Journal*, Vol. 30, No. 2, 1992, p. 403.

[12]Alrefai, M., and Acharya, M., "Controlling Leading-Edge Suction for the Management of Unsteady Separation over Pitching Airfoils," AIAA Paper 95-2188, June 1995.

[13]Petot, D., "Differential Equation Modeling of Dynamic Stall," *Recherche Aerospatiale*, No. 5, 1989, pp. 59–72.

[14]Peters, D. A., "Toward a Unified Aerodynamic Model for Use in Rotor Blade Stability Analysis," 40th Annual Forum of the American Helicopter Society, Arlington, VA, May 1984, pp. 525–538.

[15]Narendra, K., and Annaswamy, A., *Stable Adaptive Systems*, edited by T. Kailath, Information and System Sciences Ser., Prentice–Hall, Upper Saddle River, NJ, 1989, pp. 141–144.

[16]Kailath, T., *Linear Systems*, Prentice–Hall, Upper Saddle River, NJ, 1980, pp. 260–264.